Optimization of Controllable Deformation Zone And Die Wear of Aluminum Crown Forgings For Shock Absorber Assembly

Hui-Zhen Su
National Central University
Ming-Hsiu Ho
National Central University
Jyun-Kai Shih
National Central University
Cheng-Fu Huang
GLOBAL TEK.
Hao-Yun Ku
GLOBAL TEK.
Chien-Wei Chan
GLOBAL TEK.
Yiin-Kuen Fuh (michaelfuh@gmail.com)
National Central University

Research Article

Keywords: Controllable deformation zone, Crown for shock absorber assembly, Finite element method, Response surface method, Wear depth

Posted Date: September 21st, 2021

DOI: https://doi.org/10.21203/rs.3.rs-888637/v1

Abstract

In this research, numerical analysis, response surface method (RSM) and experiments are used to investigate and verify the hot forging process for manufacturing aluminum crown forgings for shock absorber assembly. First, establish the computer aided design (CAD) model of the die and the billet, and simulate it from the finite element method (FEM). Second, a new preforming die was designed with a preformed dressing of controllable deformation zone (CDZ) by the CAD software. Third, numerical simulation was combined with RSM to optimize the processing parameters with the aim of minimizing the die wear while the integrity of forgings should be prioritized preserved. According to RSM, the billet size and preformed dressing of CDZ are important factors affecting the distance between die and workpiece (C). The optimal design factor of the preforming die: billet diameter (D), billet length (L) and flash design (F) are 40 mm, 205 mm and CDZ 1, respectively. Through the results of FEM, this study describes the distribution of microscopic grain flow lines are highly related to forming, stress, strain, and temperature as well as die design such as CDZ in preformed dressing. In order to accurately verify that the parameters analyzed by the RSM, both numerical analysis and physical experiments are carried out and optimal scheme exhibit reasonable consistency.

Introduction

The CDZ study of the hot forging die shows that the material loss and the change of the geometric shape indicate the effectiveness of the hot forging die and whether there are defects in the forging die [1–4]. Tool life has a significant influence on material costs, forging process and post-processing. Several studies show the analysis of the failure and damage of forging tools [5–6]. The molding equipment in the hot forging process will be due to friction and wear, thermal fatigue, plastic deformation and brittle cracks of the mold [1]. If the forging die is deformed, its surface combination and density will change [7–9]. The pressure per unit area and the friction of the contact surface, the hardness of the material and the quality of the forging will all affect the mechanical load of the forging. The die forging process mainly involves expanding its effectiveness to reduce the life of forging tools [10–12]. The most effective way to increase the life of forging tools is to surface treatment for forging dies [13–17].

Besides, combining finite element analysis (FEA) is a method to enhance rationality and research efficiency. The finite element method (FEM) estimates mold wear and compares finite element modeling results with experimental data to ensure the reliability of this model [18]. The Archard abrasive application model is usually used to simulate the forging process and adjudge the qualitative and quantitative changes in the geometry of forging tools [19–20]. A number of studies have shown that trying to adjust the wear described by the Archard model to a practical mechanism without considering the applicable wear mechanism [21–23]. For radial forging of shafts or pipes, FEM can be used to analyze the influence of the mold joint on the deformed cross-section [24]. The mold design that increases the fillet groove or the draft angle can improve the life of the mold and the filling of the forging [25]. By designing a movable flash gap on the forging die, experiments and FEA confirmed that the movable flash gap significantly affects the material flow [26]. So as to improve the precision of hot

forged gears, a forging die shrink-fit design can be used. This method has been verified by experiments and FEM realization [27]. Optimized the die structure and process parameters for beam forming and provide a lot of support; the results show that the filling performance of half-wall die forgings has been significantly improved [28]. A method for optimizing the blank and forging die is proposed, eliminating the groove defects and describing the shortcomings of forging, such as insufficient filling, hide laps or stress, etc. [29]. It is shown that the deficiency is highly correlated with the contact area between the tube and the two molds [30]. The preforming die and hot forging process can be adjusted and optimized through the Marc software, and the die set with the best performance has been obtained [31]. Multiple rows of sprockets are produced using a semi-precision die, and then the influence of speed on cavity filling is analyzed [32]. The new closure proposed to eliminate the existing steering knuckle forming process is the extrusion forging die [33]. The most severe cause of mold failure mechanism is thermomechanical fatigue [34].

There have been many experimental cases using design of experiment (DOE) methods to optimize processing parameters, for instance, full factorial design [35–37], Taguchi method [38–40], Analysis of variance (ANOVA) [41–42], and fuzzy logic [43–44]. According to previous studies, the most effective way to improve material flow and increase die filling is to optimize the forging die geometry. The influence on the internal quality of cast SAE305 alloy parts is analyzed by the DOE method, and the best process parameters have been obtained [45]. The Taguchi method utilizes to study the effect of forming parameters on density castings, and the optimized parameters were confirmed [46]. Taguchi and FEM are used for forging molds of large and complex straight bevel gears to improve cavity filling and improve mold replacement [47]. Using the Taguchi method to improve the plastic injection molding process parameters, and the mixed use of GA-PSO and RSM can reduce time and cost, and obtain high-quality parts [48]. Utilize Taguchi method to combine CAD technology to optimize the drawing die with multiple objectives, and the structure of the lower die was increased [49].

In this paper, FEM and RSM are collocated to optimizing the forging of crown for shock absorber assembly. This method is legitimate arithmetic to increase the accuracy and efficiency of the experiment. Research and industry often use DOE to optimize the process and reduce the actual operation cost and time. The numerical simulation includes the filling rate of forgings, material flow, effective stress, strain, etc., for analysis and verification of its rationality. Thence, a preformed dressing is presented to increase the accuracy of the crown for shock absorber assembly in this research.

Die Design Of The Crown Forging

3.1 Original die design

In order to improve the efficiency and reduce the time effective method, according to the forging die, the forging die is designed by combining the shape and size of the part with CAD/CAE technology.

According to the requirements of the forging process, designing the forging die as a combination of CAD technology and the geometry and size of the forging, which is an effective method to reduce the time and enhance the efficiency. The steps of forging a crown forging are as follows. First, preforming and finishing according to the relevant parameters of the crown forging. Second, determine the hot forging sequence to distribute the billet. Third, determine the cavity parameters. As shown in Fig. 1a, the geometric dimension of forging in transverse, longitudinal, and thickness directions (A, B, C) are in the range of 180–200 mm, 60–65 mm, and 70–75 mm, respectively. The cross-section view of crown forging is shown in Fig. 1b.

The diagram in Fig. 1c shows a CAD schematic diagram of the billet used for the crown forging. The billet diameter is 40mm, the billet length is 205mm, and the billet volume is 257141mm^3. The crown forging is made of aluminum alloy 6061 and the weight is about 708g. However, the volume of the crown forging is 208613mm^3. Generally, the volume of flash accounts for 18.87% of the volume of the billet.

Figure 2 shows the geometry characteristics of the finishing die and the flash design of the top die. As shown in Fig. 2a, the flash design value of B1 is 8mm, which is deliberately specified equal-spaced around the circumferential of the forgings. Another flash design value of B1-1 is 20mm, which is deliberately designated as a damping wall (L1 = 8mm, W1 = 3mm, T1 = 4.5mm) is shown in Fig. 2c, d. In order to limit the outflow of the axial metal on the left and right sides of the crown forging cavity. When the forging material flows, the flash design prevent metal from flowing too fast and allows the excess metal to be confined in the cavity. As shown in Fig. 2b, the bottom of finishing die differs from preforming die for the geometric feature of a small bump.

Figure 3 describes that the design of the die needs to combine the shape and size of the parts with CAD/CAE technology, and then reduce the depth of the cavity, increase the length of the cavity, which improve the filling of the cavity. Then, damping walls are designed on both sides of the crown forging cavity. The damping walls are used to inhibit the outflow of metal, which enhances the filling rate of the forgings. As shown in Fig. 3a, the flash design value of B2 is 16mm, which is deliberately specified equal-spaced around the circumferential of the forgings. Compared with the finishing die when the forging material flows, the flash design is longer to confine the excess metal in the cavity and impede the metal from flowing out of the cavity quickly and generating too much waste. As shown in Fig. 3b, on the left and right sides of the crown forging cavity with damping walls are designed to restrain metal from flowing out. The dimensional characteristics of the damping walls are L = 142mm, W = 2mm, T = 3mm, shown in the enlarged drawing of the bottom die in Fig. 3c, d.

3.2 Original scheme analysis of FEM

As shown in Fig. 4a, (i) forging a round bar crown billet with a diameter of Ø40mm into a shaped billet to obtain a preliminary volume distribution; (ii) bending the billet into a prefabricated shape for preforming forging; (iii) The finishing billet is formed into a preforming part with the required metal distribution through the finishing forging; (iv) The step of completing the preforming shape is a forging operation completed on a 1000 tons mechanical forging press of crank type. In this step, the finishing forging is

completed. (v) Trimming the finishing forging is the final forged product. The actual forging is shown in Fig. 4b.

Figure 5a shows the schematic diagram of the top die and the bottom die assembled on the Chin Fong WF2-1000 mechanical crank forging press with a total capacity of 1000 tons. The heating device directly heats up the die with a gas torch. The die is made of heat-treated JIS SKD61 tool steel. The die has been heat-treated to strengthen the die and increase the life of tool. Figure 5b shows a schematic diagram of the Qform simulation of the preforming die.

Table 1
The parameters of the forging process of the crown forgings

Parameters	**Unite**	**Value**
Billet temperature	°C	480
Die temperature	°C	130
Material of billet	/	AISI Aluminum alloy 6061
Material of die	/	JIS SKD61
Heat transfer coefficient (billet to die)	kw/m^2 °C	3
Friction factor	/	0.3
Velocity of top die	Stroke/minute	90
Element style	/	Tetrahedron
Mesh size of billet	mm	1
Mesh size of dies	mm	1–16
Mesh number		100,000-200,000

Table 1 lists the simulation parameters of the hot forging process in FEM setting. The mechanical forging press of crank type 10MN was modeled in the Qform software database. The billet uses the flow stress of AISI aluminum alloy 6061 in the Qform database. The temperature of initial billet is set at 480°C. The material of forging die is set to JIS SKD61. The temperature of the forging die is set at 130°C. The coefficient of friction between the forging die and the workpiece is 0.3. The heat transfer coefficient (die to die) is set to 3 kW / m^2°C.

Equilibrium equation:

$\sigma_{ij,j} = 0$ (1)
Constitutive equation:

$$\dot{\varepsilon}_{ij} = \frac{\dot{\bar{\varepsilon}}}{\bar{\sigma}} \sigma'_{ij} \quad (2)$$

where $\bar{\sigma}$ is the equivalent stress and $\dot{\bar{\varepsilon}}$ is the effective strain rate.

Shear friction model equation:

$\tau_f = mk$ (3)

Where τ_f is the friction stress, m is the friction factor, and k is the shear yield stress limit.

Archard wear model equation:

$$W = \int K \frac{P^a V^b}{H^c} dt \quad (4)$$

where P is the normal pressure of the contact surface, V is the wear volume, H is the hardness of die(53HRC), and K is the friction coefficient (0.3), while a, b and c are material dependent constant

As shown in Fig. 6, the original geometric dimensions of the billet diameter and length is 38mm and 193mm, respectively. Similar geometric dimensions of the billet are consistent for Figs. 8 and 9. The maximum load of the preforming is 2.21MN, and the finishing maximum load is 1.74MN. The large preforming load is due to the uneven flow of the metal formed by the billet, so a large load is generated during the forming.

As shown in Fig. 7a, the diameter of the billet used is 40mm and the length is 193mm. The experimental result is that the forging is completely filled except for the right and left sides, which is marked with dotted red square. Figure 7b shows that the used billet has a diameter of 40mm and a length of 205mm. The preforming forging shows that the crown forging is completely filled (dotted cyan square), which is the best formability forging.

Figure 8 shows that the wear of the preforming is homogeneous. As shown in Fig. 8a, the mean wear depth of top die is 4.43E-5mm per forging step. The bottom die mean wear depth is 5.31E-5 mm per forging step, as shown in Fig. 8b. The geometric change of the billet in the bottom die is relatively large, which results in a comparatively high die wear.

As shown in Fig. 9, when the finishing, a large geometric change occurs on the top die, which causes a higher value of die wear to progress on the top die. The die mean wear value of top die is 1.05E-5 mm per forging step, and the die mean wear value of bottom die is 9.33E-6 mm per forging step.

As shown in Fig. 10a, the diameter of the billet used is 40mm and the length is 200mm. The simulation result is that the crown is completely filled except for the right and left sides, which is marked with dotted red square. Figure 10b shows the crown is absolutely filled. The diameter of the billet used is 40mm and the length is 205mm. Consequently, except for the different size of the billets, the other setting conditions are the same as the previous analysis conditions, so as to find the best analysis conditions.

3.3 The preforming die design with controllable deformation zone of damping walls

The cross-sectional view of the die design with controllable deformation zone is shown in Fig. 11a. The FEA results show that the initial die design makes the left and right crowns for shock absorber assembly not completely filled is shown in Fig. 11b. As shown in Fig. 11c, d, in order to ensure the high precision of the crown forging, two relating designs of controllable deformation zone with preformed dressing of CDZ 1 and CDZ 2, respectively. The value of L1 in the die design of CDZ 1 is 22 mm, and the value of L2 in the die design of CDZ 2 is 25 mm. The variable of flash design will be described in Sect. 4.

Optimized Die Of The Cdz Of Damping Walls

Since production experience is usually used to design crown forging die, the accuracy of the die cannot be guaranteed. Therefore, this research combines production experience, mathematical methods, and FEM technology to design and optimize crown forging preforming die design.

As show in Fig. 11 for the new preforming die scheme, the variables are the executed billet diameter (D), billet length (L) and flash design (F). However, the corresponding target is the distance between the preforming die and the workpiece (C). Table 2 lists the value range of each variable. In addition, flash design (F) variables include three cases of initial design without damping wall and two relating designs of controllable deformation zone with preformed dressing of CDZ 1 and CDZ 2, respectively. The reason for three level of flash design (F) value in Table 2 is primarily attributed to the design consideration practical application. In reality, flash design (F) is very complex phenomena and highly depending on experience, several modification steps are essentially inevitable after mold tryout. The proposed one level of flash design (F) value of “damping wall” is the potentially implemented way to enhance the material filling. Other complicated process involves the whole mold refurbish was not considered in this paper.

Table 2
The variable value range of preforming die

Variable	Unit	Lower-line	Median-line	Upper-line
Diameter (D)	mm	40.0	40.5	41.0
Length (L)	mm	205	206	207
Flash design (F)	/	NO-CDZ	CDZ 1	CDZ 2

Table 3
Experimental schemes and simulation results

Scheme	Factor 1 Billet diameter (D) mm	Factor 2 Billet length (L) mm	Factor 3 Flash design (F)	Target Distance between die and workpiece (C) mm
1	40.0	206	CDZ 2	0.2084
2	41.0	206	CDZ 2	0.3230
3	41.0	205	CDZ 1	0.3154
4	40.5	205	NO-CDZ	0.2757
5	40.0	207	CDZ 1	0.2206
6	41.0	207	CDZ 1	0.3484
7	40.5	207	NO-CDZ	0.2944
8	40.0	206	NO-CDZ	0.2156
9	41.0	206	NO-CDZ	0.3407
10	40.5	206	CDZ 1	0.2609
11	40.5	206	CDZ 1	0.2618
12	40.5	206	CDZ 1	0.2613
13	40.0	205	CDZ 1	0.1966
14	40.5	207	CDZ 2	0.2814
15	40.5	205	CDZ 2	0.2495

In order to obtain the best target response results, 15 groups were established through the Box-Behnken design. Qform is used to simulate each scheme and additionally, the mean values of distance between die and workpiece (C) were statistically chosen as shown in Table 3.

According to the least square method and simulation results, the equation is obtained by RSM using the fitting function between the factors (D, L, F) and the target (C). Eq. (5) can predict the distance between die and workpiece.

Distance between preforming die and workpiece equation:

$$C = 308.7 - 1.706\,D - 2.694\,L - 0.491\,F + 0.01118\,D^2 + 0.00612\,L^2 + 0.00780\,F^2 + 0.00450\,DL - 0.00525\,DF + 0.00330\,LF \quad (7)$$

Table 4
Variance analysis of the distance between die and workpiece

Factor	Sum of square	Freedom	Mean squares	F-value	P-value	
Model	0.031963	9	0.003551	479.42	< 0.001	Significant
D	0.029561	1	0.029561	3990.50	< 0.001	
L	0.001447	1	0.001447	195.36	< 0.001	
F	0.000514	1	0.000514	69.33	< 0.001	
DL	0.000020	1	0.000020	2.73	0.159	
DF	0.000028	1	0.000028	3.72	0.112	
LF	0.000044	1	0.000044	5.88	0.060	
D^2	0.000029	1	0.000029	3.90	0.105	
L^2	0.000138	1	0.000138	18.7	0.008	
F^2	0.000224	1	0.000224	30.29	0.003	
Residual error	0.000037	5	0.000007			
Correlation coefficient		$R^2 = 0.9968$				

The variance analysis of the distance between the preforming die and the workpiece is shown in Table 4. Based on RSM, the influence of this factor is significant, and the P-value must be less than 0.05. Through model variable analysis (distance between die and workpiece), the P value is less than 0.01. However, this model is significant and effective. The factors D, L, F, L^2, and F^2 in the model have a significant effect on the distance between the preforming die and the workpiece. Table 4 lists the correlation coefficient of 0.9968, indicating that the distance between the preforming die and the workpiece model has accuracy and good fit.

Fig.12 shows the important factors in constructing the statistical significance derived from the statistical analysis of the 3D response surface graph. In these three factors (process parameters): billet diameter, billet length and flash design, when one parameter is constant, the function of the other two factors is studied.

Figure 13 illustrates the main effects plot (MEP) of the three factors on the response variable of distance between preforming die and workpiece. The vertical axis represents the average value of C in micrometers, and the horizontal axis is divided into three parts for each factor, and each level of the factor is shown in its own unit. However, when the D is 40mm, the average value of C is 0.203mm; when the L is 205mm, the average value of C is 0.258mm; when the F is CDZ 1, the average value of C is 0.262mm. In order to obtain the optimized factor, the minimum distance between the preforming die and the workpiece should be selected. From the above, the optimized factor is D: 40mm, L: 205mm, F: CDZ 1.

Result And Discussion

Table 5
The optimal scheme of design

Variable	Value
D	40mm
L	205mm
F	CDZ 1

First of all, the target to be achieved is that the forging must be completely filled. The optimized scheme described in Sect. 4 is that the billet diameter is 40mm, the billet length is 205mm, and the flash design as CDZ 1, as shown in Table 5. The distance between die and workpiece is zero, which is equivalent to a fully filled forging.

As shown in Fig. 14 of contact ratio (100% corresponds to the distance between die and workpiece is zero), the cavity of the crown forging is well filled. In order to conform the filling conditions of the left and right sides of the crown marked with red circles, the cavities filled with different forging steps are shown in Fig. 14. It is recognized that the left and right sides of the crown are fully filled in step 253 with contact ratio of 100%.

The diagrams in Fig. 15 illustrates the maximum loads of the preforming and finishing are 5.59 MN and 3.41 MN, respectively. Compared with the original design (as shown in Fig. 6), the optimized design increases the forging load by 60.47%, while the finishing load increases by 48.97%. Due to the increase in the diameter and length of the billet, the forming load becomes larger, but it improves the problem of filling defects, which are very important to the forging quality.

Figure 16 shows the optimized preforming dies mean wear depth of the crown forging. The preforming die mean wear depth per stroke is 6.64E-5 mm is shown in Fig. 16b. The severely worn area is located in the middle of the bottom die. Consequently, the flash design increases the mean wear depth of the die per stroke, which is in good agreement with the RSM analysis of Fig. 12. In comparing with the original design of the wear depth of each die and the size of the billet, due to the increase in the diameter and length of the billet, the average wear depth of each die of the upper and lower dies increased by 36.74% and 25.05%, respectively.

The diagram in Fig. 17 shows that the wear depth of the finishing die is uniform, and the wear is distributed around the forging die cavity. The average wear depth per stroke of the finishing top die is 1.62E-5 mm is shown in Fig. 17a. Compared with the wear depth of the initial finishing die, the average wear depth per stroke depth of the finishing top and bottom die increased by 35.19% and 49.98%, respectively. Therefore, the optimization of the preforming has a significant impact on the mean wear depth per stroke of the finishing die.

Figure 18 illustrates the color nephograms of the finishing forging of a crown forging including damage, plastic strain, effective stress and temperature. The damage indicates the location where the forging is prone to defects, as shown in Fig. 18. The diagrams in Fig. 18a shows the damage of the billet is uniformly transformed, and severe areas of damage appear in the flash, which is difficult to produce defects on the crown forging. Plastic strain denotes the degree of deformation in the deformation process of the billet. Figure 18b shows that the area of plastic strain is particularly increased from the junction of the crown forging and flash, which results in effective strain accumulation due to the greater resistance to metal flow in the flash area in the cavity. Therefore, in order to ensure the filling of the cavity, generally increasing the damping walls is an effective method. In Fig. 18c, the maximum effective stress region is in the junction of the crown forging and the flashlight. Consequently, the right and left sides of the crown are not easy to deform, and the CDZ is conducive to the filling of the cavity on both sides of the crown. Figure 18d shows that the maximum temperature reaches approximately 508℃. Since the material is concentrated on the corners, the highest temperature appears at the junction of the crown forging and the flashlight. Figure 18b verifies this in reverse. The temperature of the workpiece rises due to the heat generated during forging. In Fig. 18e, the velocity is uniformly distributed in the crown forging, and the maximum velocity occurred in the flash area. The diagrams in Fig. 18f illustrates the displacement is uniform, and the maximum displacement occurs in the cavities on both sides of the crown forging and flash.

Figure 19 demonstrates that the discussion of the effect of preformed dressing on the crown forging, the points tracking of the right crowns for shock absorber assembly. Figure 19a shows the cross-sectional view of the left and right crowns of the shock absorber assembly is red circled in Fig. 14. Because of insufficient filling of the left and right crowns of the shock absorber assembly (as shown in Fig. 10), six points are marked to investigate the effect of the damping wall in CDZ. In Fig. 19b, c, the effective stress point trend tracking and plastic strain point trend tracking are different according to the amount of change of the forging. The greater the amount of change of the forging, the greater the effective stress. However, the effective stresses of P4 and P5 are greater than other effective stresses. Figure 19d shows the velocity point tracking is periodic fall and rise; Thus, the tendency has been consistently justified. Figure 19e states that the temperature tracking trend is regular before the die stroke 20mm, but the temperature tracking trend at P4 and P5 is lower than other temperatures after the die stroke 20mm. Due to P4 and P5 are the fastest to contact the die cavity, and the die temperature is lower than that of the billet material, so P4 and P5 will experience the steepest temperature gradient as contrasted with other points. The temperature induced effect will inevitably inhibit the metal flow due to higher interfacial friction so the forming load will be higher, as well as the effective stress and plastic strain of the material will increase.

The production equipment for crown forging is shown in Fig. 20. The bending equipment is shown in Fig. 20a, it is 110 tons C-frame single crank power presses. Figure 20b illustrates the use of a high-frequency induction heated the billet after bending to the preforming equipment. The huge crank press is used to forge crown forging, which can provide 1000 tons of pressure, preforming and finishing forging as shown

in Fig. 20c-d. Figure 20e shows a 60-ton C-frame single-crank power press, which is used to trim the flash of forging.

Eventually, through the air-cooled, the crown forging is shown in Fig. 21a. The diagram in Fig. 21b shows the actual bottom die is designed with RSM optimized damping walls (L = 142mm, W = 2mm) on the left and right sides of the crown forging cavity to increase the filling effectiveness of the forging and prevent excess metal from flowing out. Figure 21c shows the finite element simulation results (left) and experimental results (right) of the grain flow lines distribution after forging. As shown in Fig. 21d and Fig. 21e, a partially enlarged view shows the left side of the actual forging (blue square), in which the crystal grain streamlines of the forging are densely and orderly distributed. The grain flow lines at the bottom of the trench gradually form uniform flow lines along the edge of the trench, which is consistent with the finite element simulation result (orange square). Therefore, experimental grain flow lines distribution shows smooth and non-intersecting dense flow lines which is consistent with the simulation counterparts.

Conclusion

In this article, insufficient filling often occurs in the crown forging with the critical focus on deformation mechanism of controllable deformation zone and die wear of Aluminum Alloy forgings. The three-dimensional finite element model of the optimized performed dressing of damping wall is analyzed by using commercially available FEM software Qform 3D to establish and design of experiment. RSM can explore and explain that complex variables will affect the target response variable to obtain the best response target, and then use three-dimensional finite element to provide detailed information about die wear, forming load, and whether the forging is completely filled. This information is incorporated into the process design. Draw the following conclusions from the final results:

(1) First of all, the requirement is high-precision forgings, and we use experimental design methods to design three billet diameters and three billet lengths. The FEM verified that the optimal size was Ø40 mm, 205 mm, which can make the forging complete filling, and it is actually verified that this billet size can completely filled the forging.

(2) In RSM, the P value of the contact distance model between the mold and the workpiece is less than 0.05, and the correlation coefficient (R-sq) is, which is a highly significant model. Among the three factors, the P values of D, L, and F are less than 0.05, indicating that these three factors have a significant impact on the model.

(3) Compared with the original die design, the other two related designs of controllable deformation zone with preformed dressing of CDZ 1 and CDZ 2, respectively. Based on the response surface method and experimental verification, it is shown that CDZ 1 can effectively improve the filling of crown forgings. It can be seen that the preforming die to be repaired has an important influence on the accuracy of crown forgings.

(4) The FEM simulation results show that the integrated billet diameter is 40mm, the billet length is 205mm and the flash design as CDZ 1. The plastic deformation is evenly distributed, which can significantly improve the formability and filling rate.

Declarations

Ethical approval

Since the study is performed at a relevant lab, there is no need for ethical approval. Additionally, the paper's main data is not published elsewhere.

Consent to participate

All authors declare that have agreed for authorship, have read and approved the manuscript, and have given the consent for submission and subsequent publication of the manuscript.

Consent to publish

All authors are consenting to publish this article with its included data in The International Journal of Advanced Manufacturing Technology and approve its final version.

Authors' contributions

All authors contributed equally to the generation and analysis of experimental data, and the development of the manuscript.

Funding

This work was financially funded by Global Tek.

Competing interests

The authors declare that they have no competing interests.

Availability of data and materials

The authors confirm that the data supporting the findings of this study are available within the article.

References

1. Gronostajski Z, Kaszuba M, Hawryluk M, Zwierzchowski M. A review of the degradation mechanisms of the hot forging tools. Arch Civil Mech Eng 2014;528–539
2. Hawryluk M. Methods of analysis and increasing durability of forging tools used in hot die forging processes, monographic publishing series. Problems of operation and machine construction 2016;ISBN 978-83-7789-410-1 Ed Scientific ITE – PIB Radom

3. Hawryluk M, Mrzygłód B (2018) A durability analysis of forging tools for different operating conditions with application of a decision support system based on artificial neural networks (ANN). Eksploatacja i Niezawodno sc –. Maint Reliab 19/3:338–348
4. Gronostajski Z, Kaszuba M, Polak S, Zwierzchowski M, Niechajowicz A, Hawryluk M (2016) The failure mechanisms of hot forging dies. Mater Sci Eng A Struct Mater: Prop Microstruct Process 657:147–160
5. Ebara R, Kubota K (2008) Failure analysis of hot forging dies for automotive components. Eng Fail Anal 15:881–893
6. Paschke H, Nienhaus A, Brunotte K, Petersen T, Siegmund M, Lippold L et al. Adapted diffusion processes for effective forging dies. 21st international ESAFORM conference on material forming (ESAFORM) location (Univ Palermo, Palermo, ITALY, 1960) 2018
7. Hawryluk M, Ziemba J (2019) Lubrication in hot die forging processes. Proc Inst Mech Eng Part J J Eng Tribol 233/5:663–675
8. Barrau O, Boher C, Vergne C, Rezai-Aria F. Investigation of friction and wear mechanism of hot forging tool steels. 6th int tooling conference (Karlstadt) 2002
9. Baumel A, Seeger T (1990) Material data for cyclic loading. Supplement 1, vol 61. Elsevier Science Publishers Amsterdam, Materials science monographs
10. Gronostajski Z, Kaszuba M, Hawryluk M, Marciniak M, Zwierzchowski M, Mazurkiewicz A et al (2015) Improving durability of hot forging tools by applying hybrid layers. Metalurgija 54(4):687–690
11. Gronostajski Z, Kaszuba M, Hawryluk M, Zwierzchowski M (2014) A review of the degradation mechanisms of the hot forging tools. Arch Civil Mech Eng 14(4):528–539
12. Smolik JA (2012) Hybrid surface treatment technology for increase of hot forging dies. Arch Metall Mater 57(3):657–664
13. Altan T (2005) Cold and Hot Forging Fundamentals and Application. ASM International. Ohio State University
14. Mazurkiewicz A, Dobrodziej J. Model of intelligent database in processing of information concering data of constitution of surface layers. 4th CONTECSI - International Conference on Information Systems and Technology Management 2007
15. Babu PD, Prasannakuma B, Marimuthu P, Mishra RK, Ram Prabhu T (2019) Microstructure, wear and mechanical properties of plasma sprayed TiO2 coating on Al–SiC metal matrix composite. Arch Civil Mech Eng 19(3):756–767
16. Mazurkiewicz A, Smolik J (2015) The innovative directions in development and implementations of hybrid technologies in surface engineering. Arch Metall Mater 60(3):2161–2172
17. Gronostajski Z, Hawryluk M, Kaszuba M, Marciniak M, Niechajowicz A, Polak S et al (2016) The expert system supporting the assessment of the durability of forging tools. Int J Adv Manuf Technol 82:1973–1991

18. Behrens BA (2008) Finite element analysis of die wear in hot forging processes. CIRP Ann – Manuf Technol 57:305–308
19. Archard JF (1953) J Appl Phys 24:981–988
20. Bayer RG (2004) Mechanical wear fundamentals and testing. Marcel Dekker Inc
21. Ghorbani S, Kopilov VV, Polushin NI, Rogov VA (2018) Experimental and analytical research on relationship between tool life and vibration in cutting process. Arch Civil Mech Eng 18/3:844–862
22. Thiyagu M, Karunamoorthy L, Arunkumar N (2019) Thermal and tool wear characterization of graphene oxide coated through magnetorheological fluids on cemented carbide tool inserts. Arch Civil Mech Eng 19/4:1043–1055
23. Abachi S, Akkok M, Gokler M (2010) Wear analysis of hot forging dies. Tribol Int 43:467–473
24. Ghaei A, Movahhedy MR (2007) Die design for the radial forging process using 3D FEM. J of Mater Process Technol 182:534–539
25. Liu Y, Wu Y, Wang J, Liu S (2018) Defect analysis and design optimization on the hot forging of automotive balance shaft based on 3D and 2D simulations. Int J Adv Manuf Technol 94:2739–2749
26. Langner J, StonisM, Behrens BA (2016) Investigation of a moveable flash gap in hot forging. J of Mater Process Technol 231:199–208
27. Eyercioglu O, Kutuk MA, Yilmaz NF (2009) Shrink fit design for precision gear forging dies. J of Mater Process Technol 209:2186–2194
28. He H, Huang S, Yi Y, Guo W (2017) Simulation and experimental research on isothermal forging with semi-closed die and multistage- change speed of large AZ80 magnesium alloy support beam. J of Mater Process Technol 246:198–204
29. Jin Q, Han X, Hua L, Zhuang W, Feng W (2018) Process optimization method for cold orbital forging of component with deep and narrow groove. J Manuf Process 33:161–174
30. Oba W, Imaizumi Y, Kuboki T (2018) Two-step forming for improvement of forming limit in rotary nosing with relieved die for fabrication of axisymmetric and eccentric nosed tubes. J of Mater Process Technol 262:350–358
31. Liu J, Cui Z (2009) Hot forging process design and parameters determination of magnesium alloy AZ31B spur bevel gear. J of Mater Process Technol 209:5871–5880
32. ChengW CC, Wang Y, Lin P, Zhao R (2015) LiangW. 3D FEM simulation of flow velocity field for 5052 aluminum alloy multirow sprocket in cold semi-precision forging process. Trans Nonferrous Met Soc China 25:926–935
33. Zhou J, Lin L, Luo Y (2014) Themulti-objective optimization design of a new closed extrusion forging technology for a steering knuckle with long rod and fork. Int J Adv Manuf Technol 72:1219–1225
34. Gronostajski Z, Marcin K, Sławomir P, Maciej Z, Adam N, Marek H (2016) The failure mechanisms of hot forging dies. Mater Sci Eng A 657:147–160
35. Ahn SH, Montero M, Odell D, Roundy S, Wright PK (2002) Anisotropic material properties of fused deposition modeling ABS. Rapid Prototyp J 8:248–257

36. Chin KA, Leong KF, Chua CK, Chandrasekaran M (2006) Investigation of the mechanical properties and porosity relationships in fused deposition modelling- fabricated porous structures. Rapid Prototyp J 12:100–105
37. Onwubolu GC, Rayegani F (2014) Characterization and optimization of mechanical properties of ABS parts manufactured by the fused deposition modelling process. Int J Manuf Eng 2014:13
38. Anitha R, Arunachalam S, Radhakrishnan P (2001) Critical parameters influencing the quality of prototypes in fused deposition modelling. J Mater Process Technol 118:385–388
39. Chohan JS, Singh R (2016) Enhancing dimensional accuracy of FDM based biomedical implant replicas by statistically controlled vapor smoothing process. Prog Addit Manuf 1:105–113
40. Wang CC, Lin T, Hu S. Optimizing the rapid prototyping process by integrating the Taguchi method with the Gray relational analysis. Rapid Prototyp J 2013
41. Lee BH, Abdullah J, Khan ZA (2005) Optimization of rapid prototyping parameters for production of flexible ABS object. J Mater Process Technol 169:54–61
42. Nancharaiah T (2011) Optimization of process parameters in FDM process using design of experiments. Int J Emerg Technol 2:100–102
43. Sahu RK, Mahapatra SS, Sood AK (2013) A study on dimensional accuracy of fused deposition modeling (FDM) processed parts using fuzzy logic. J Manuf Sci Prod 13:183
44. Huynh HN, Nguyen AT, Ha NL, Thu T, Thai H. Application of fuzzy taguchi method to improve the dimensional accuracy of fused deposition modeling processed product. Int Conf Syst Sci Eng 2017:107–12
45. Verran GO, Mendes RPK, Valentina DLVO (2008) DOE applied to optimization of aluminum alloy die castings. J of Mater Process Technol 200:120–125
46. Syrcos GP (2003) Die casting process optimization using Taguchi methods. J of Mater Process Technol 135:68–74
47. Qi Z, Wang X, Chen W (2019) A new forming method of straight bevel gear using a specific die with a flash. Int J Adv Manuf Technol 100:3167–3183
48. Chen WC, Nguyen MH, Chiu WH, Chen TN, Tai PH (2016) Optimization of the plastic injection molding process using the Taguchi method, RSM, and hybrid GA-PSO. Int J Adv Manuf Technol 83:1873–1886
49. Lin BT, Kuo CC (2011) Application of the fuzzy-based Taguchi method for the structural design of drawing dies. Int J Adv Manuf Technol 55:83–93

Figures

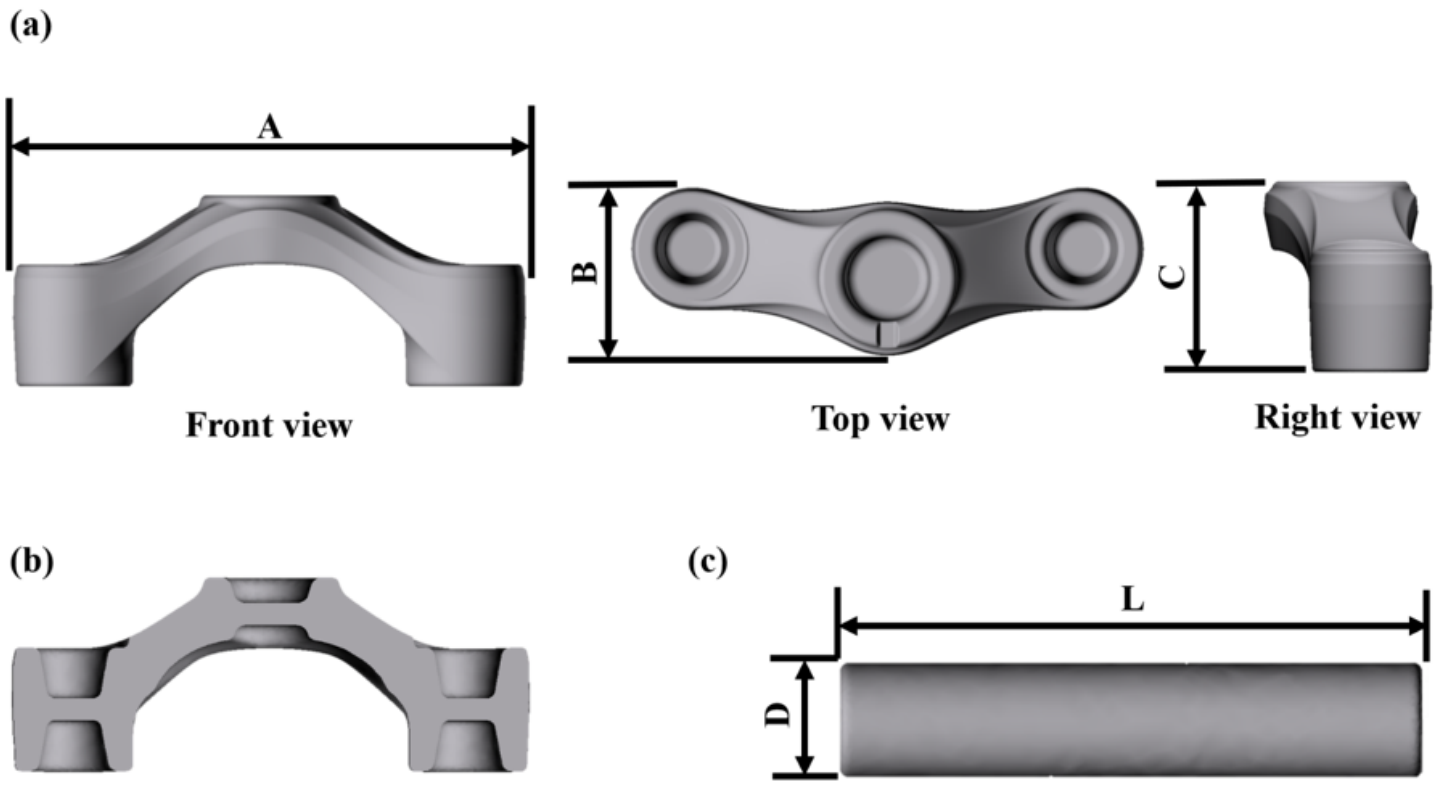

Figure 1

The targeted component dimension and initial workpiece dimension for the crown forging. a CAD models with front, top, right view. b The cross-section view of crown forging c billet.

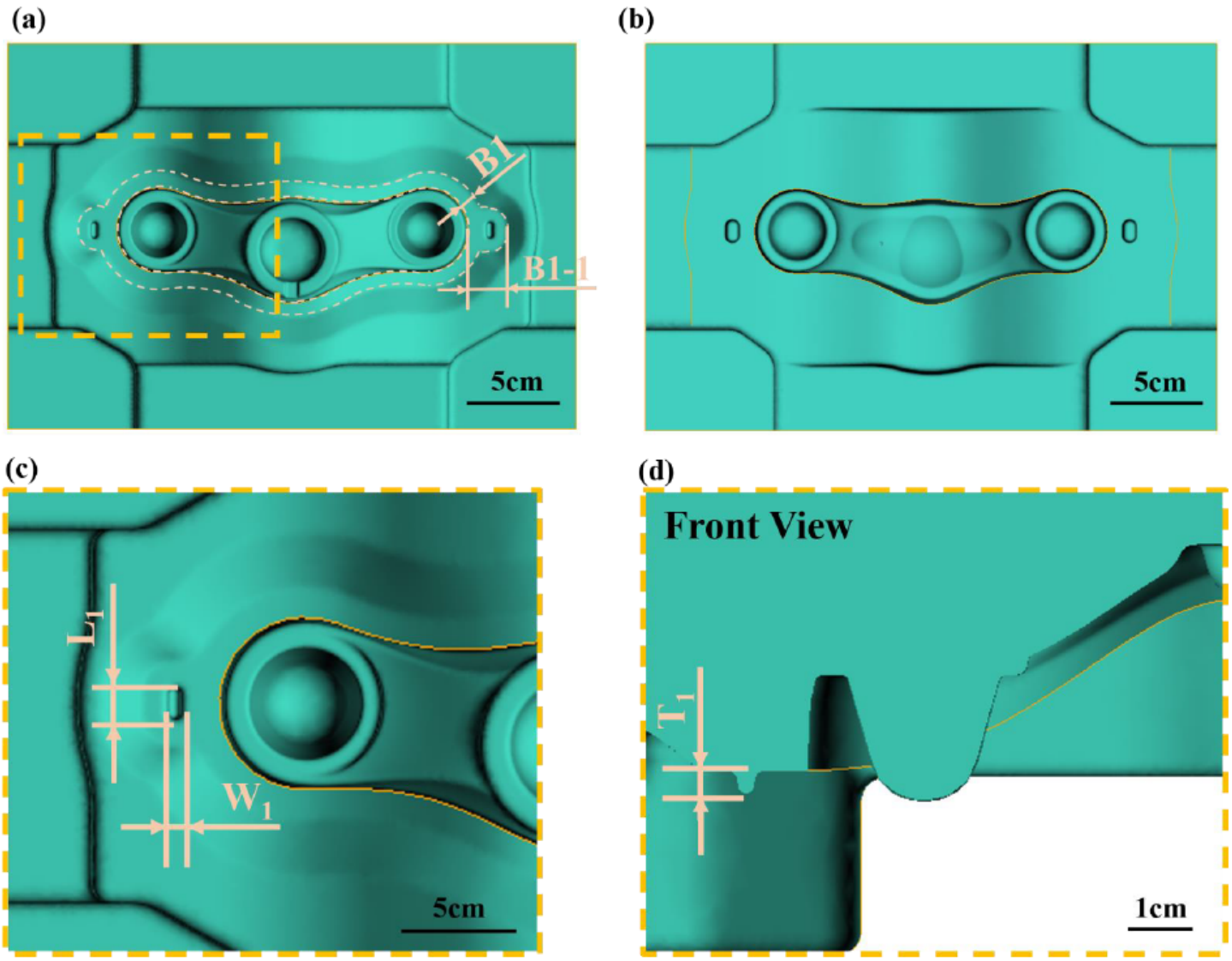

Figure 2

Original design of finishing dies. a Top die. b Bottom die. c Partial enlarged view of top die d Partial enlarged front view of top die

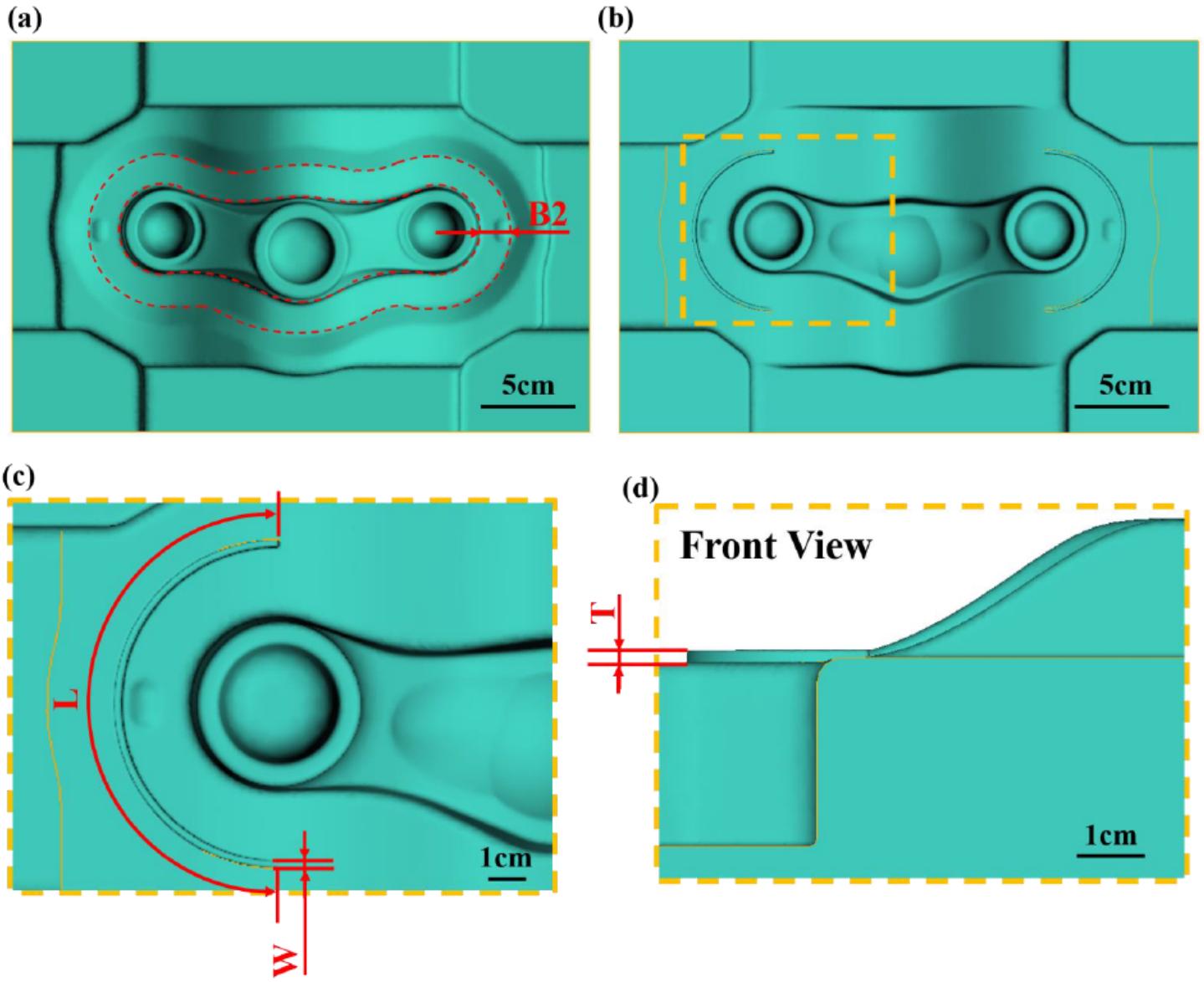

Figure 3

Original design of preforming dies. a Top die b Bottom die c Partial enlarged view of bottom die d Partial enlarged front view of bottom die

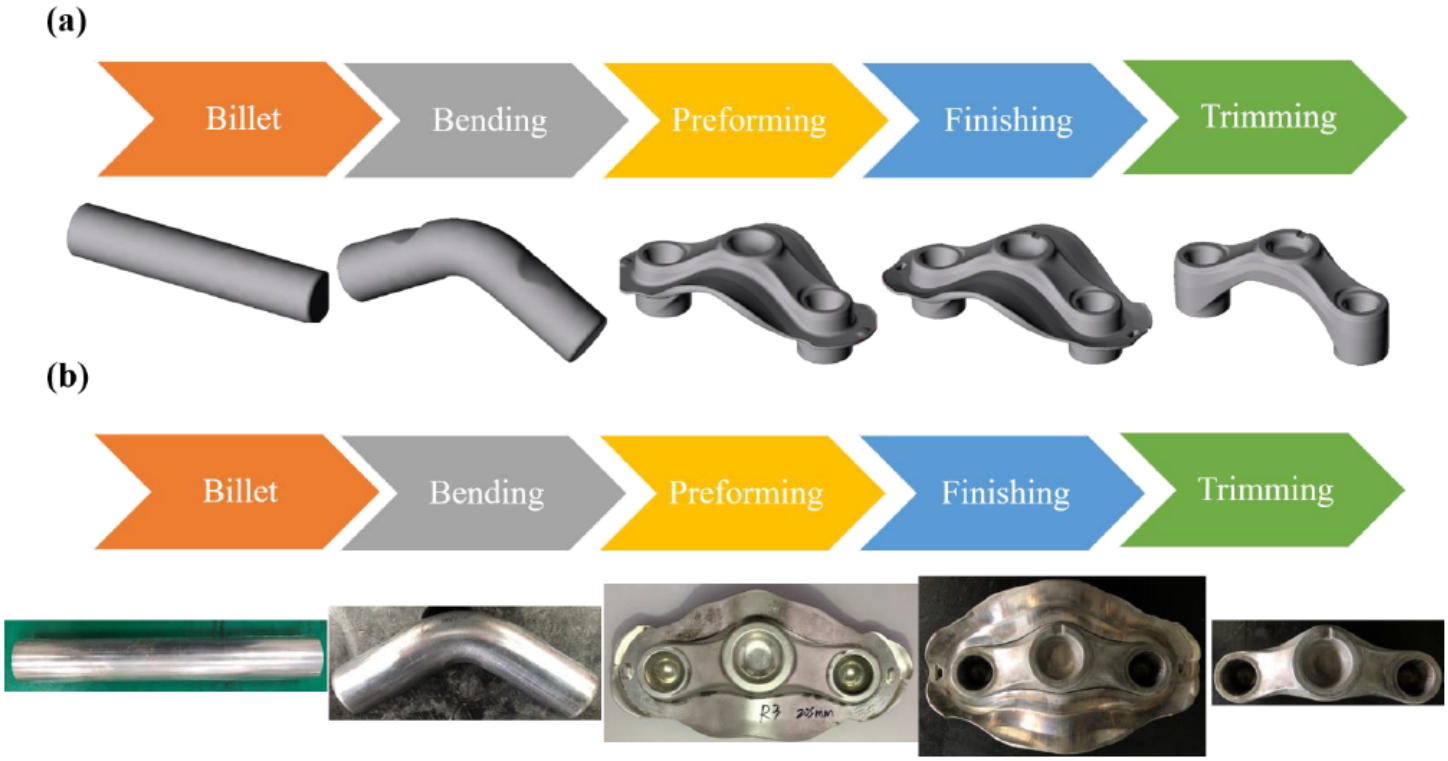

Figure 4

Process design. a FEM model b The actual forging.

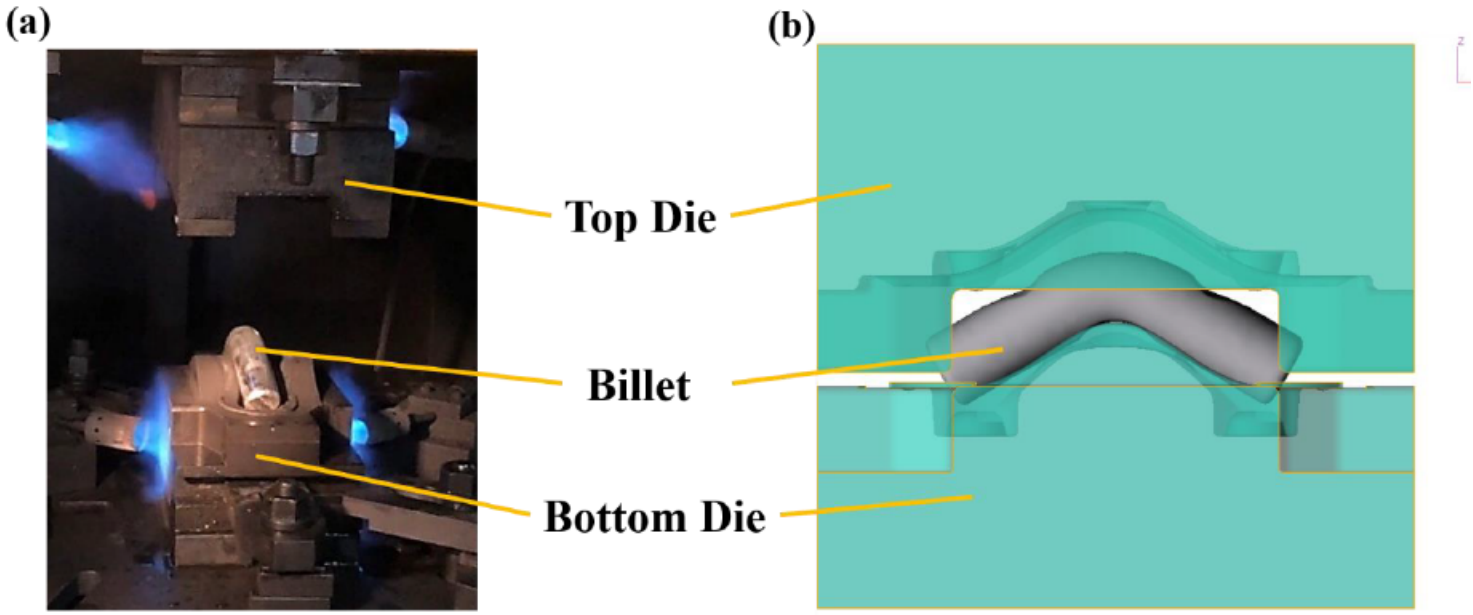

Figure 5

Preforming die design. a The actual forging die. b FEM model in Qform simulation.

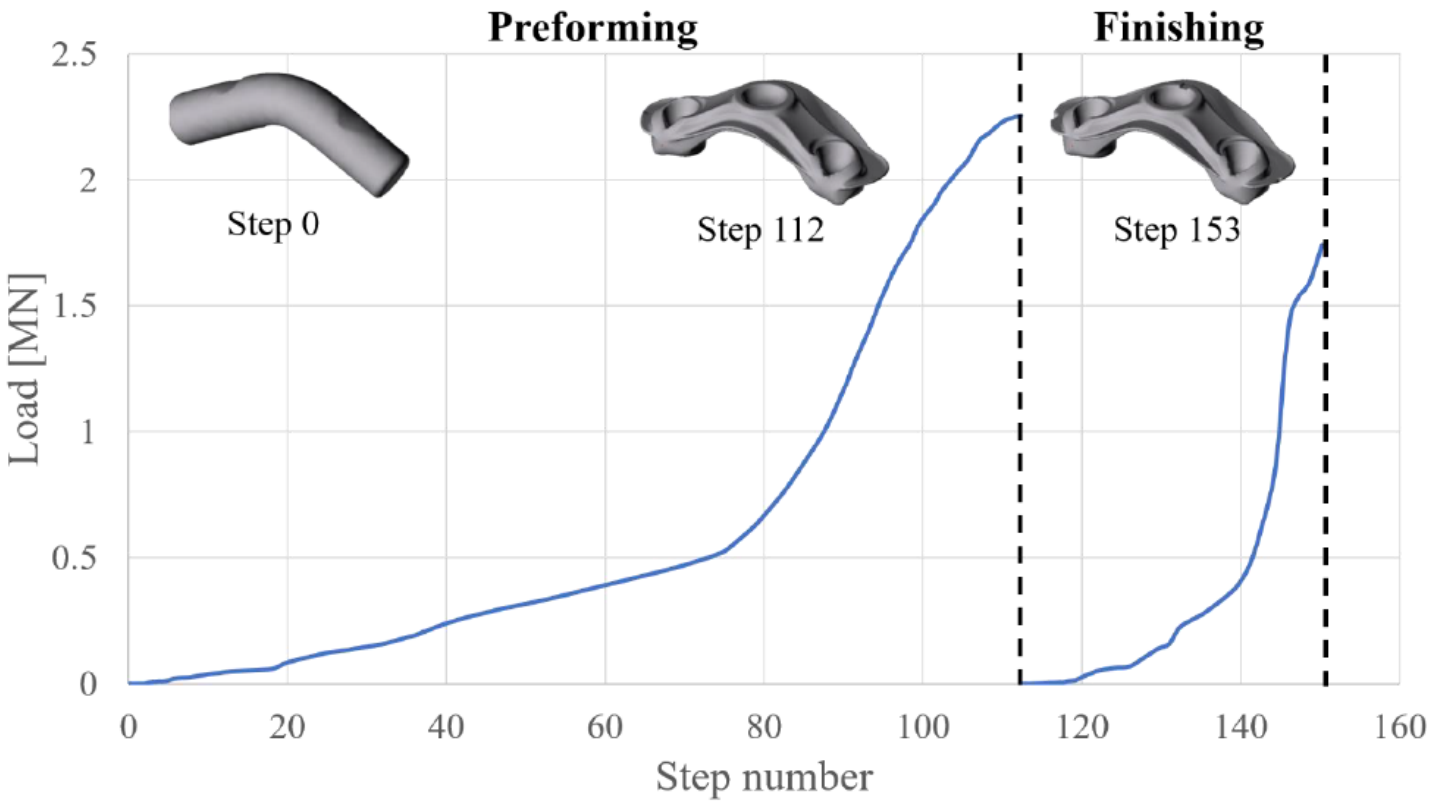

Figure 6

Hot forging load by initial die design.

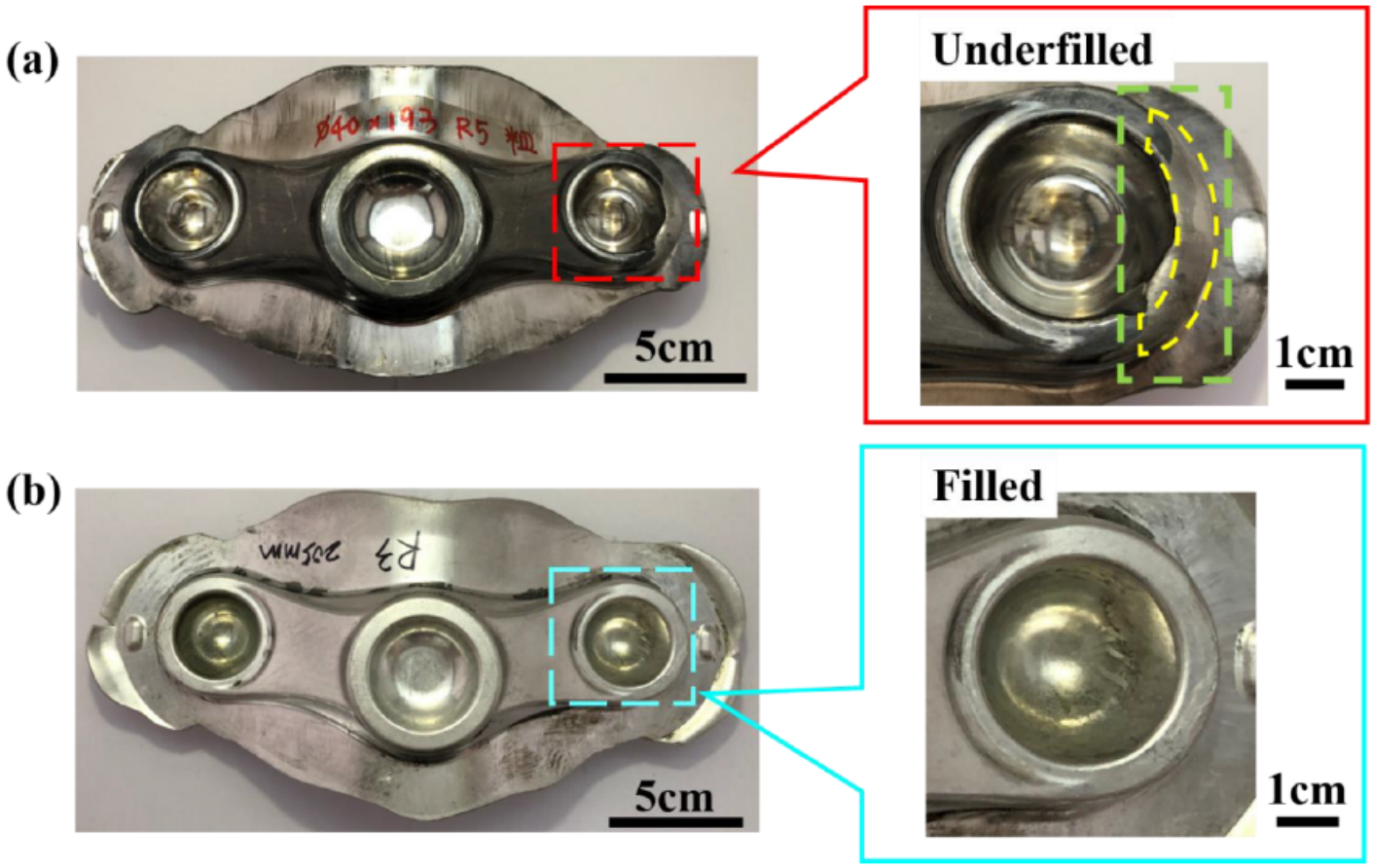

Figure 7

The experimental results. a the NG forging. b the good forging.

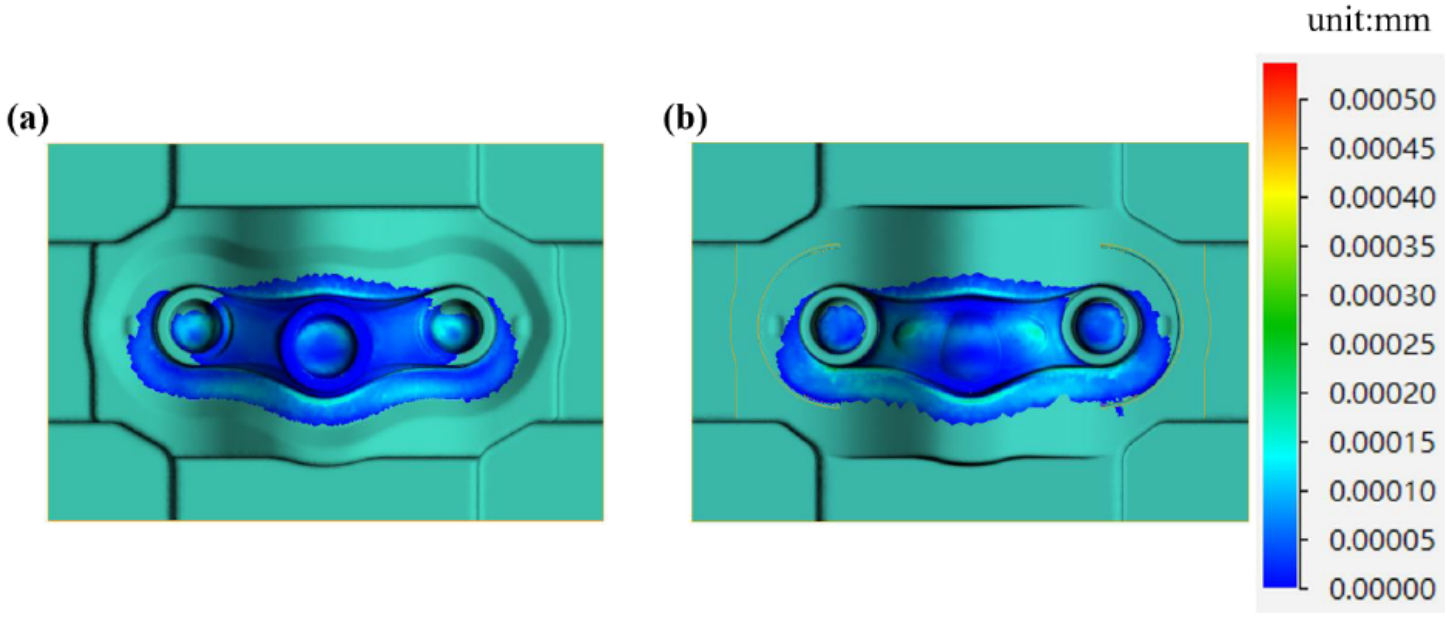

Figure 8

The mean wear depth of original designed preforming dies. a Top die. b Bottom die

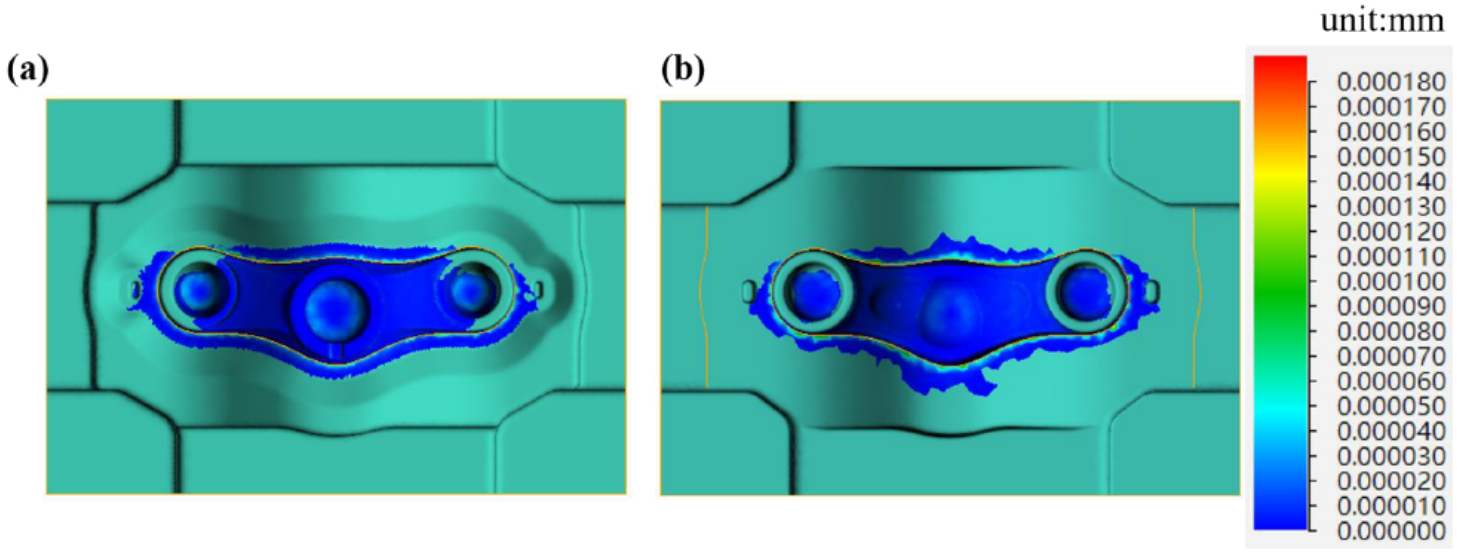

Figure 9

The mean wear depth of original designed finishing dies. a Top die. b Bottom die

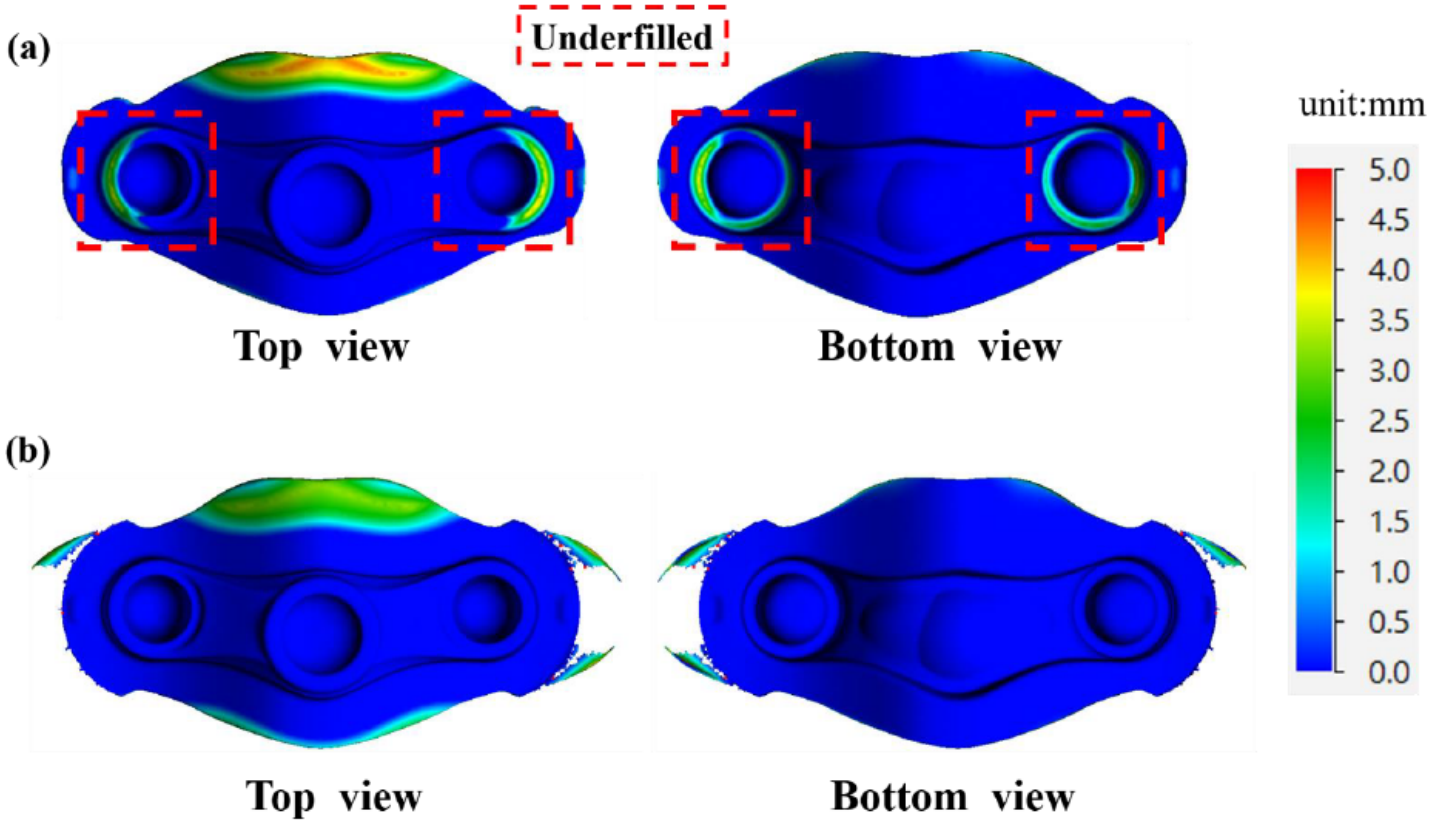

Figure 10

a The underfilled behavior of smaller billet scheme (Ø40mm and L200mm) as illustrated by distance to contact. b The filling behavior of bigger billet scheme (Ø40mm and L205mm). Blue color indicates the

fully contact between the die and the forging, i.e. complete filling.

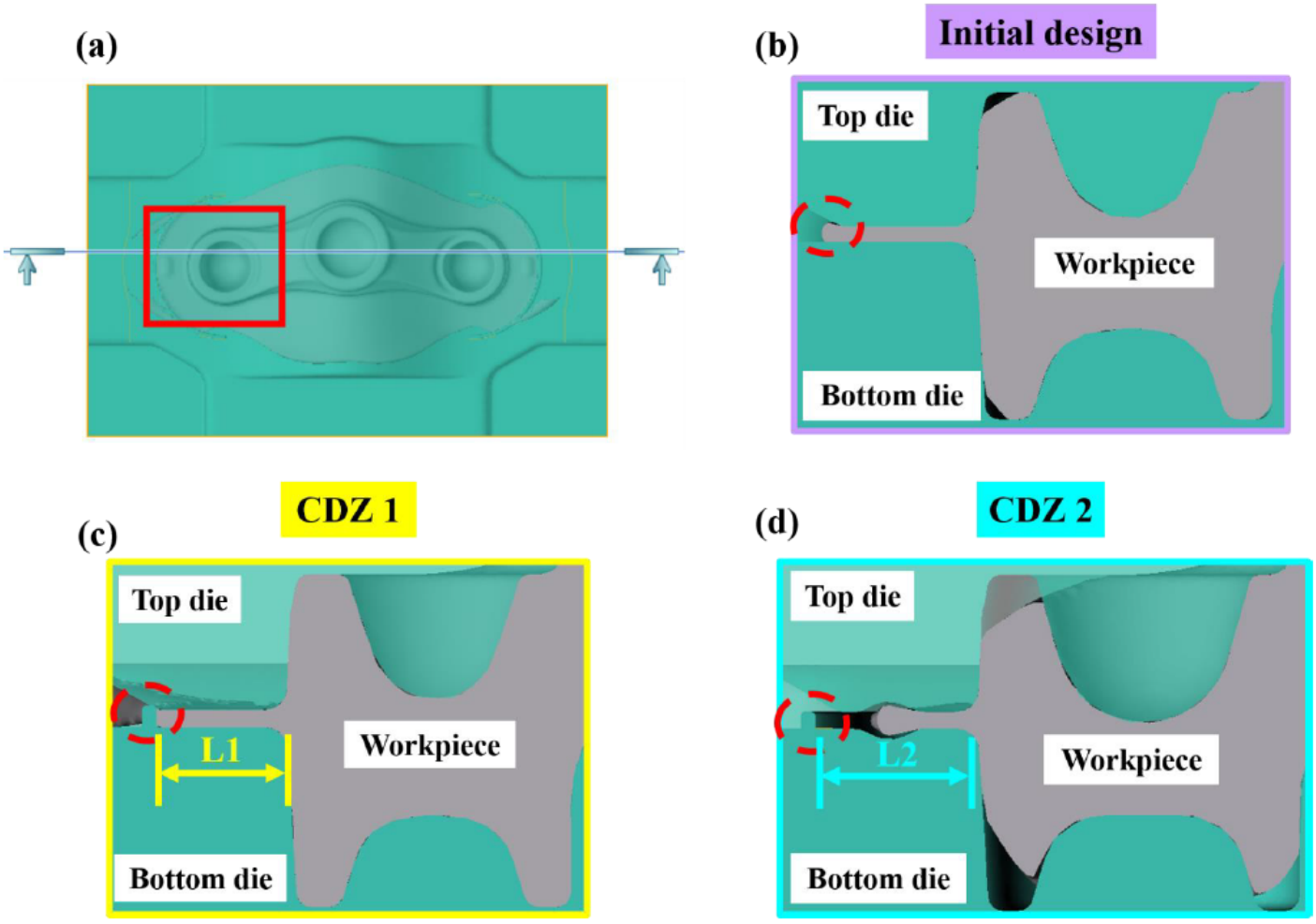

Figure 11

The preforming die optimization. a The cross-section view of crown forging. b Initial design. c CDZ 1. d CDZ 2.

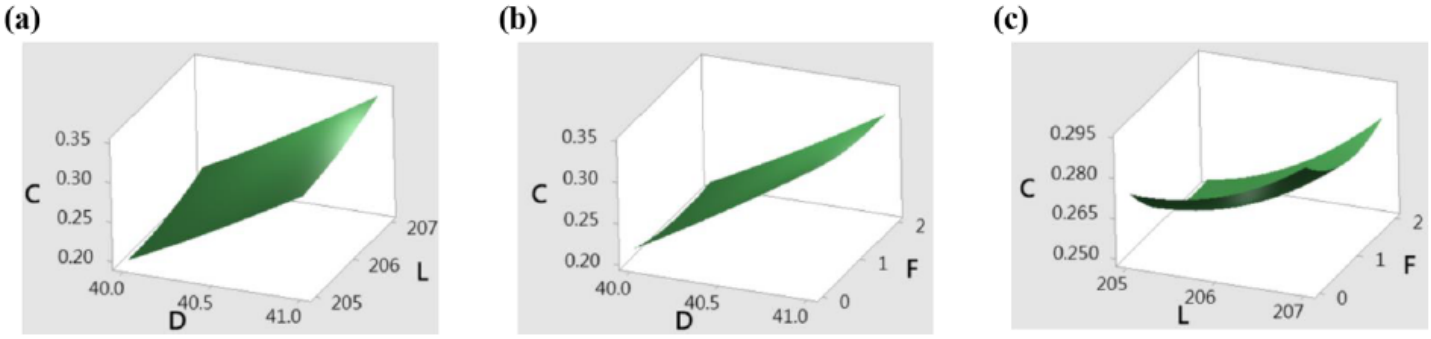

Figure 12

RSM of the minimum distance between die and workpiece

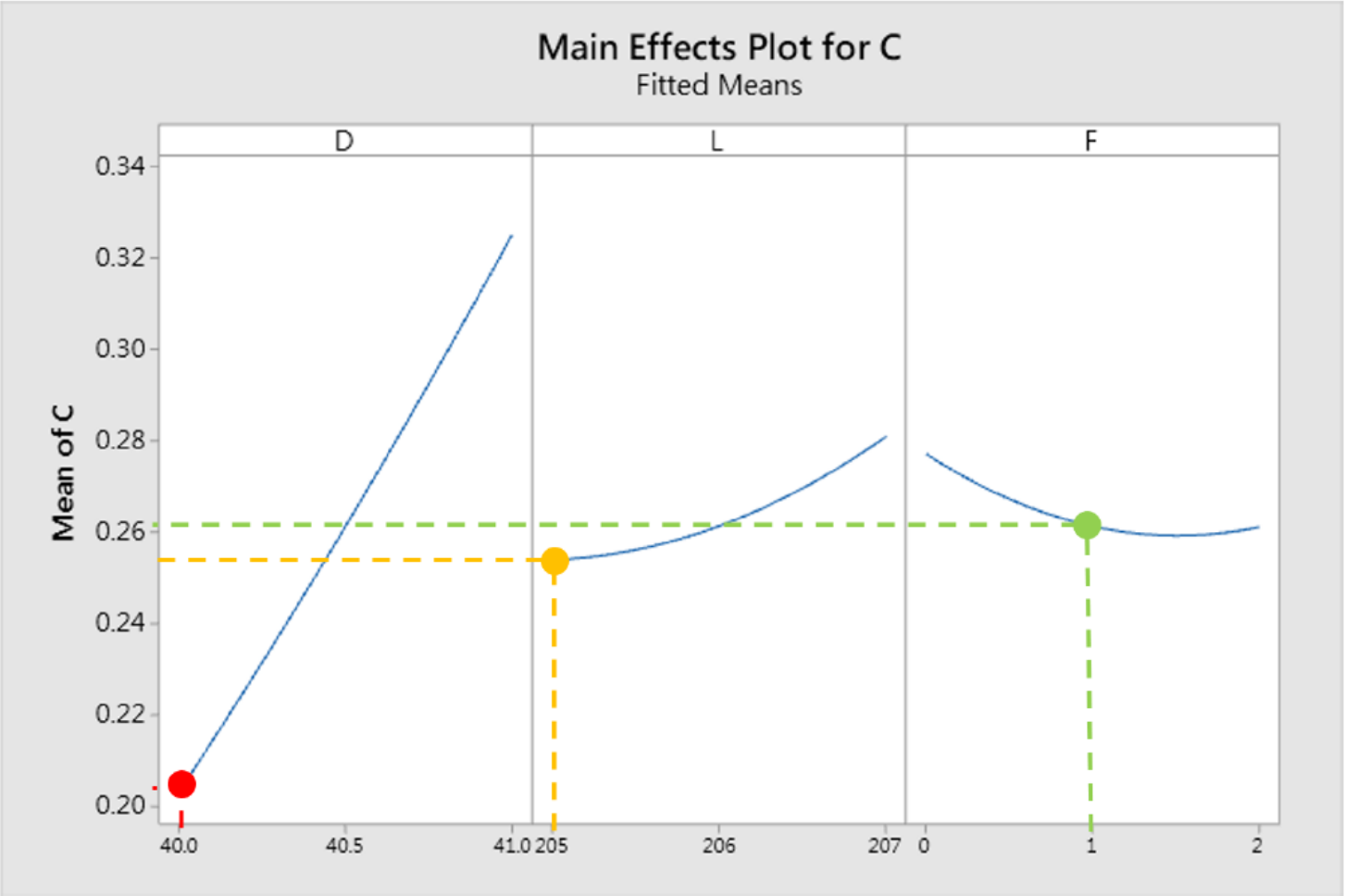

Figure 13

The Main effect plot of distance between die and workpiece

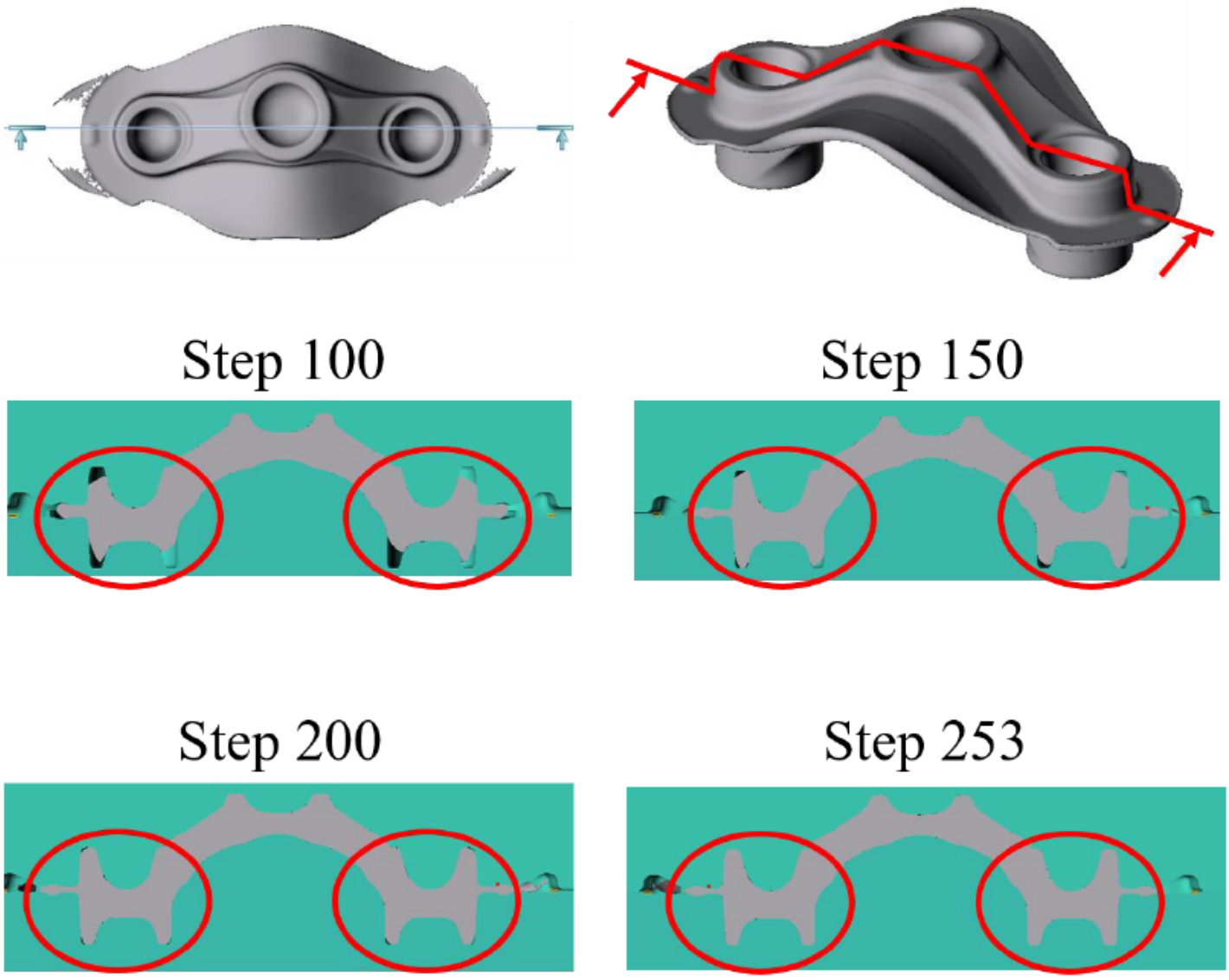

Figure 14

Contact ratio of crown forging

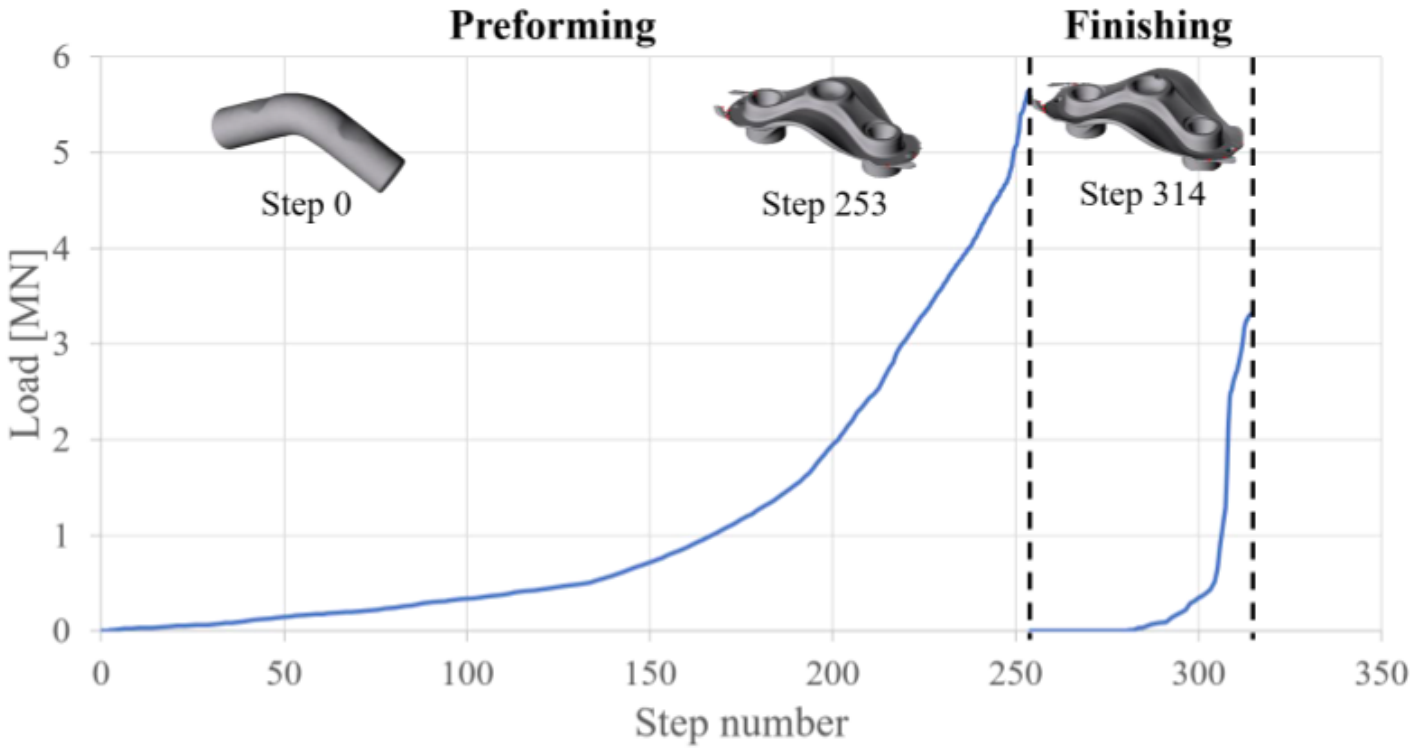

Figure 15

The forming load of optimal scheme

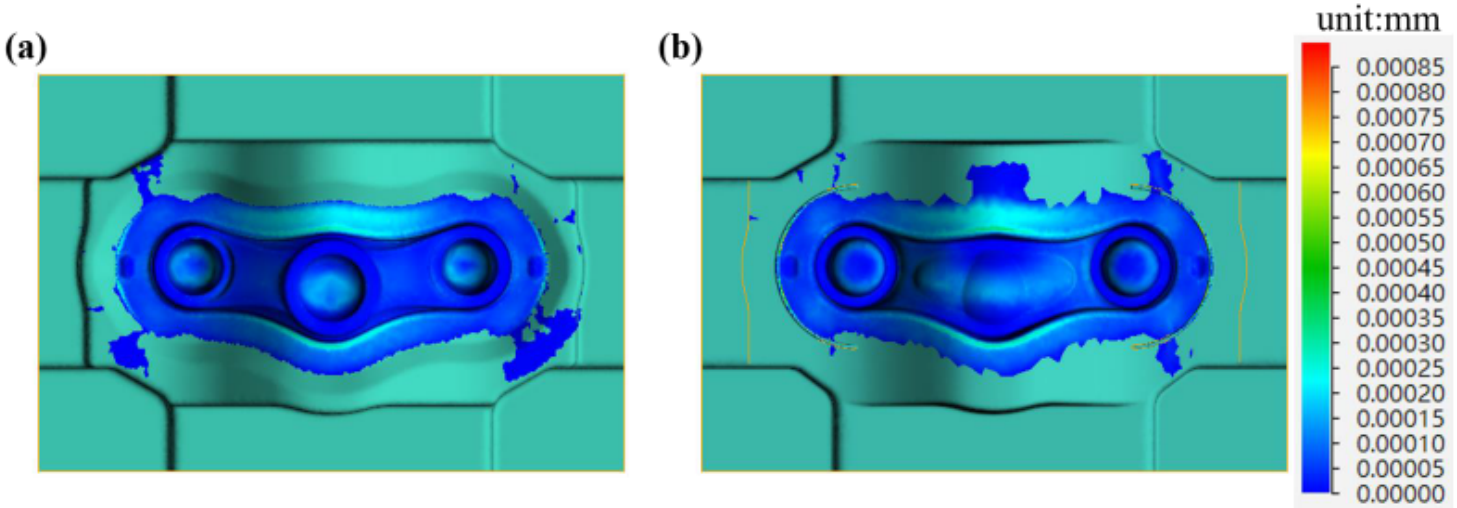

Figure 16

The preforming die mean wear depth per stroke. a Top die. b Bottom die

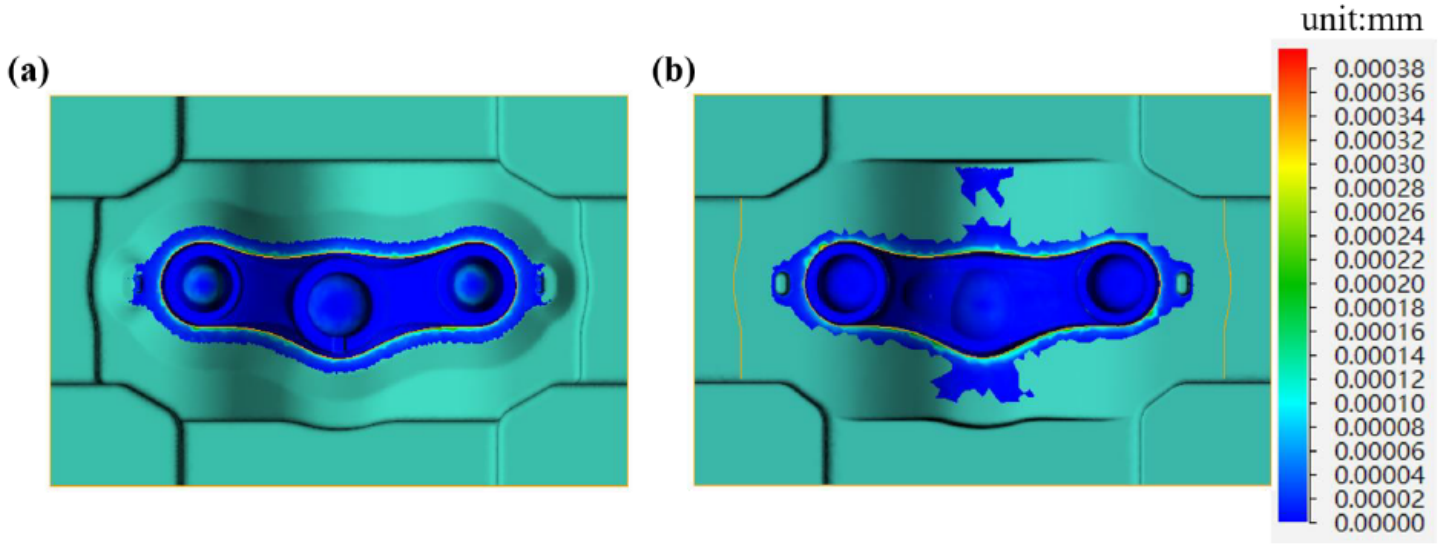

Figure 17

The finishing dies mean wear depth per stroke. a Top die. b Bottom die

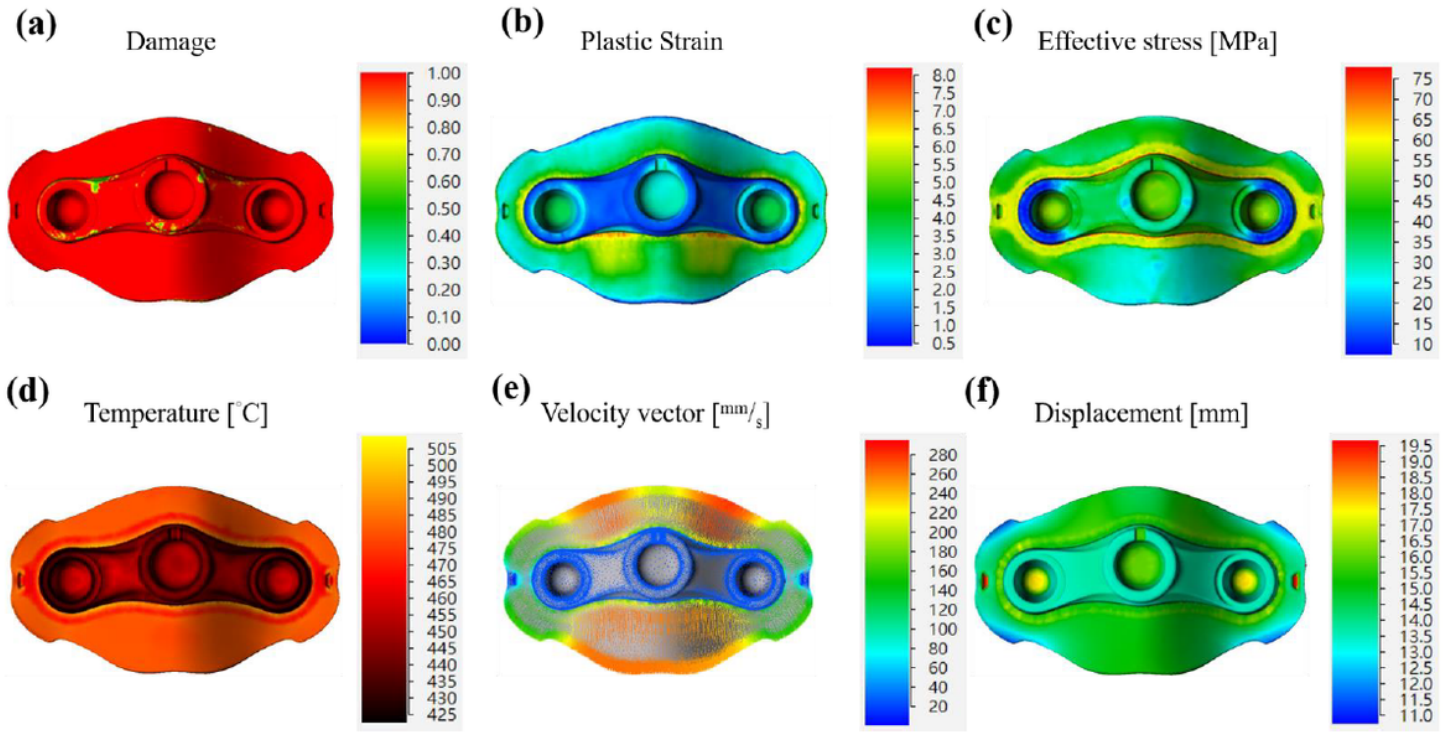

Figure 18

The finishing forging color nephograms of crown forging

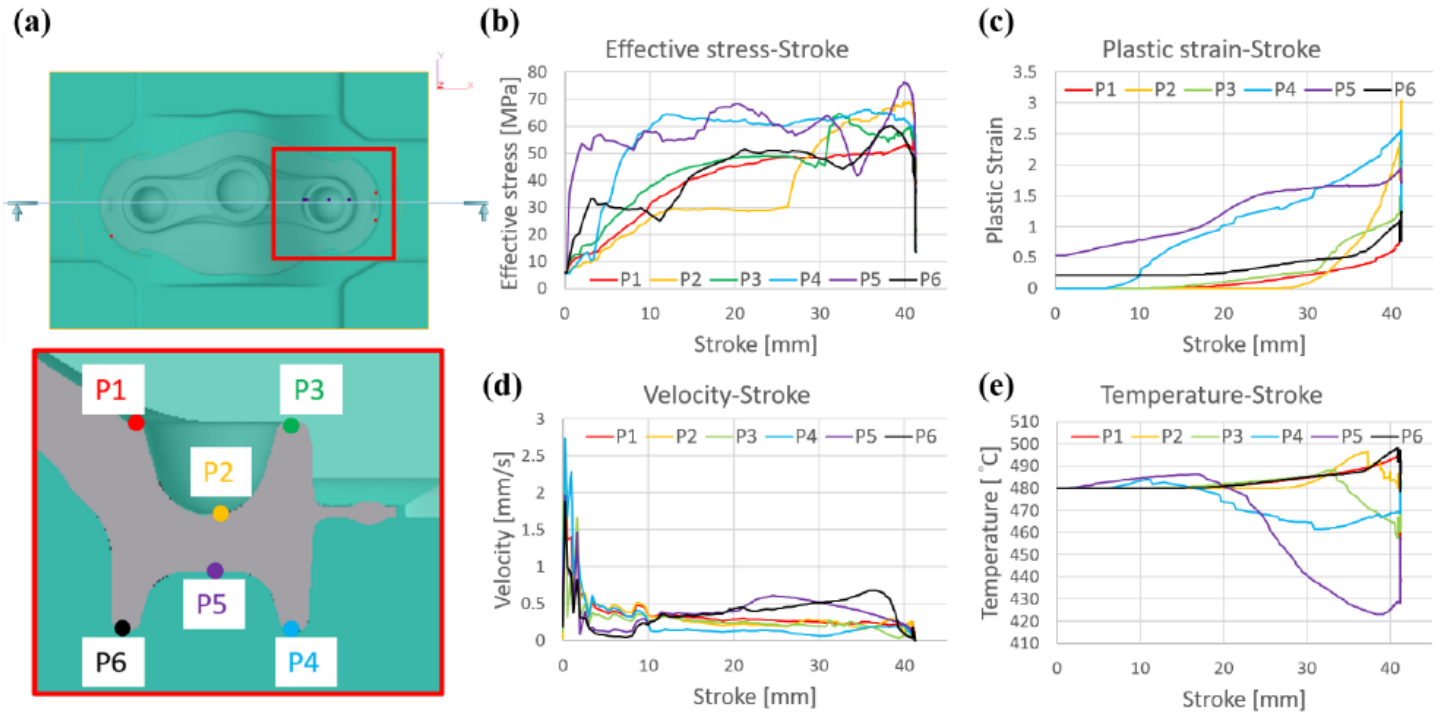

Figure 19

The points tracking of right crown for shock absorber assembly

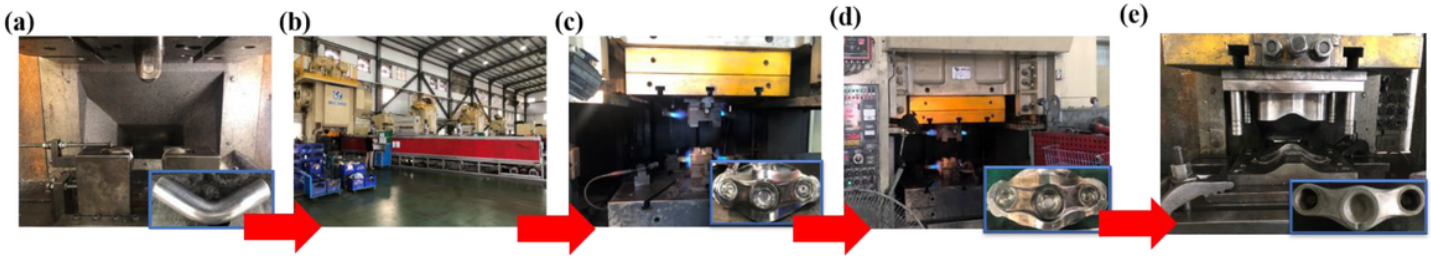

Figure 20

The production equipment of crown forging

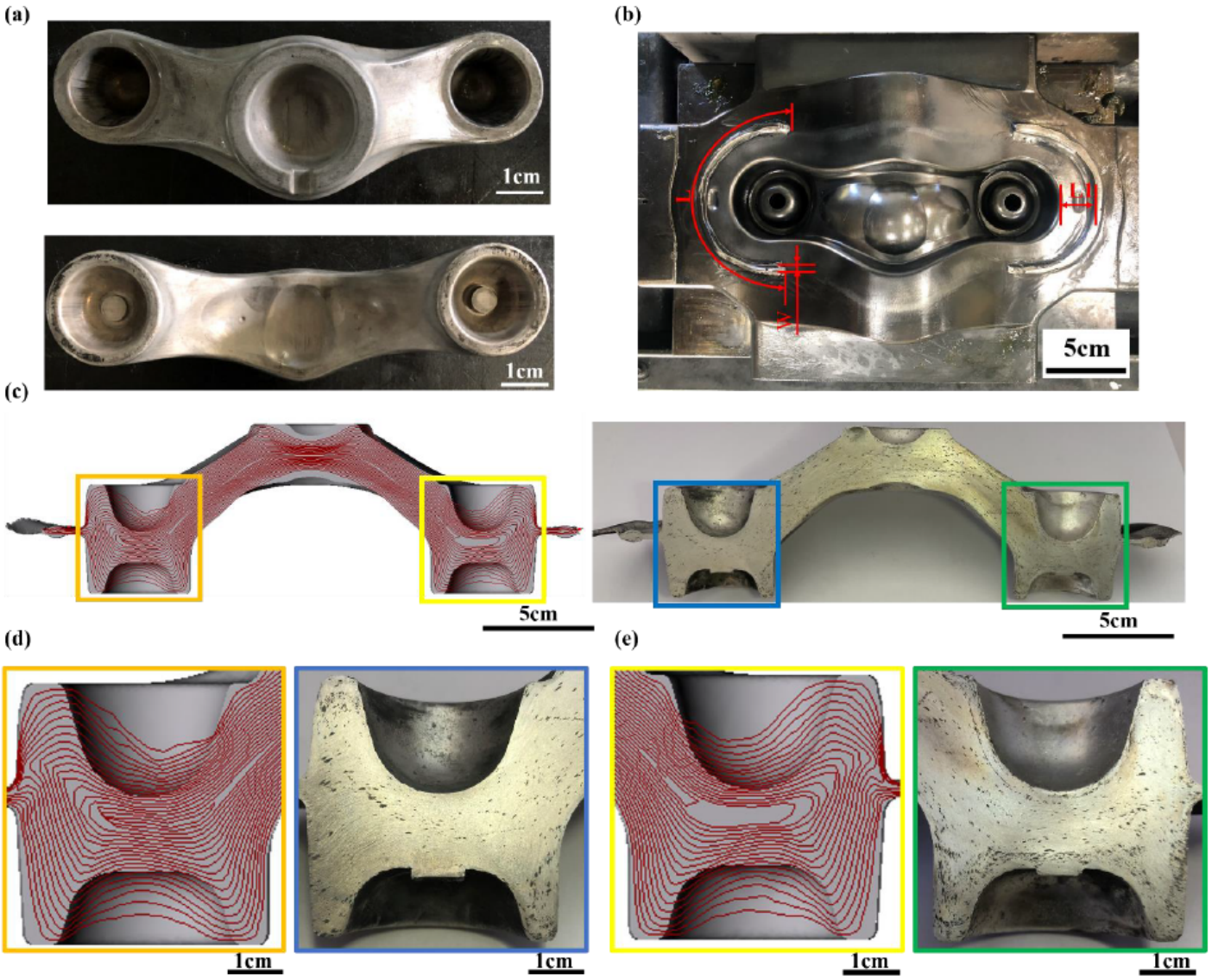

Figure 21

a The top view and bottom view of finished forging. b The actual bottom die with CDZ 1(L1=22mm). c The cross-section view of finished forging with grain flow lines. (left: simulation; right: experiment) d The partial enlarged view of left side of finished forging with grain flow lines. (orange square: simulation; blue square: experiment) e The partial enlarged view of right side of finished forging with grain flow lines. (yellow square: simulation; green square: experiment)